MOF Thin Film-Coated Metal Oxide Nanowire Array: Significantly Improved Chemiresistor Sensor Performance

*Ming-Shui Yao, Wen-Xiang Tang, Guan-E Wang, Bhaskar Nath, and Gang Xu**

As a critical family of chemiresistor materials, metal oxides (MOX), such as ZnO, SnO_2, and In_2O_3, have been developed for many industrial and domestic applications in volatile organic compound (VOC) detection due to their low cost, portability, real-time operability, and ease of use.[1] To pursue higher sensitivity, better selectivity, faster responsivity, and lower working temperature, nanostructured MOX materials have been extensively studied due to their increased surface-to-volume ratios and reactive surface areas compared with bulk.[1b,2] However, selectivity is still a major challenge for commercial MOX gas sensor devices, although several ways, such as cross-sensitivity adjustment, electronic noses and gas preseparation by other instrument, have been developed to address this issue.[3] For instance, water vapor is a typical interference of MOX gas sensor for VOC detecting, which commonly exists in the air with high concentration (40–70 RH%, ≈11 440–20 019 ppm) and will generate false responses to a major source for unreliable results.[4] Although many efforts like doping, p–n junctions, and noble metal decoration have been made to reduce the negative effects of humidity, an ideal solution is still in need.[4b,c]

Metal organic framework (MOF) is a class of crystalline framework-structured material constructed by connecting metal center with organic linker. Such materials feature regular pores, ultra large surface areas, tunable framework structures, and open-metal sites and demonstrate potential applications on catalysis, gas storage and separation, drug delivery, nanoscale reactors, proton conduction, etc.[5,6] Particularly, their selective gas adsorption behavior makes MOF very attractive for overcoming the selectivity problem in gas sensor.[7–9] For example, Zhang's group reported two hydrophobic MOFs, $[Co(im)_2]_n$ and $[Co(mim)_2]_n$, exhibiting selective response to VOC gases without the interference of humidity.[7a,b] In contrast, Achmann et al. first found that hydrophilic MOF, Fe-1,3,5-benzenetricarboxylate, selectively shows higher response to humidity than VOCs.[8] Even so, the reported MOF-based chemiresistor sensors suffer from low sensitivity to analytes.[8–10]

Dr. M.-S. Yao, Dr. G.-E. Wang, Dr. B. Nath, Prof. G. Xu
State Key Laboratory of Structural Chemistry
Fujian Institute of Research on the Structure of Matter
Chinese Academy of Sciences (CAS)
155 Yangqiao Road West
Fuzhou, Fujian 350002, P. R. China
E-mail: gxu@fjirsm.ac.cn
Dr. W.-X. Tang
Institute of Materials Science
University of Connecticut
97 N. Eagleville Road, Storrs, CT 06269, USA

DOI: 10.1002/adma.201506457

Here, we propose a new material design strategy to improve the performance of chemiresistor gas sensor by combining the high sensitivity of nanostructured MOX with the high selectivity and catalytic activity of MOF into one material. First, MOX nanowire is used as core material for gas sensing reaction and subsequent electrical signal transport. Then, by coating a layer of MOF thin film on the surface of MOX nanowire, a MOX@MOF core–sheath nanowire material could be obtained. In such a core–sheath nanostructured material, the porous sheath material is used to selectively usher desired target species and reject interfering gases from passing through to reach MOX surface. By this manner, the selectivity of MOX gas sensor could be greatly improved. Moreover, catalytic properties of MOF may also be introduced into such materials to enhance their sensing performance.

For the first time, the above described strategy was successfully demonstrated by coating a layer of hydrophobic and catalytic Zeolitic Imidazolate Framework - CoZn (ZIF-CoZn, isostructural with ZIF-8(Zn) or ZIF-67(Co)) thin film on ZnO to form a core–sheath nanowire array for chemiresistor gas sensor, which can improve the performance on detecting acetone under humidity interference. The detection of ppb/ppm-level acetone is of great essence for environmental monitoring and clinic application.[11] On one hand, acetone is one of most used solvents and reagents in industry and laboratory. It can anaesthetize the central nervous system of human and cause damage to kidney, pancreas, and liver. On the other hand, acetone is an important breath biomarker for diagnosing diabetes, because its concentration would increase from 3 to 9 ppm in health human body to more than 18 ppm in diabetic patients. Breath acetone analysis was found to be more effective than urine sampling for monitoring ketosis for insulin-dependent diabetic patients.[12] However, the humidity in environment and human breath can vary within a broad range, and the cross-sensitivity of humidity may plague the precise detection of acetone by MOX sensors due to their intrinsically poor selectivity. We found that ZnO@ZIF-CoZn nanowire array-based sensor shows greatly enhanced selectivity of acetone to humidity, much better response, accelerated response and recovery behavior, and significantly decreased working temperature, compared with ZnO nanowire array-based sensor.

The ZnO@ZIF-CoZn gas sensor was prepared by coating a layer of ZIF-CoZn thin film on ZnO nanowire array via a simple solution method (for details see **Figure 1** and Table S1, Supporting Information). Notably the synthesis of MOF-coated metal oxide nanorod has been reported by others.[13] In their work, metal oxide nanorod works as sacrificial template to supply Zn^{2+} for constructing MOF. Differently, besides Zn^{2+} dissolved from ZnO nanorod, foreign Co^{2+} source was also involved in the synthesis of ZnO@ZIF-CoZn. The competition

Figure 1. Schematic illustration of the preparation of ZnO@ZIF-CoZn gas sensors.

between Co^{2+} and Zn^{2+} to coordinate to organic ligand results the control synthesis of ZnO@ZIF-CoZn much more complex. Moreover, in order to obtain higher aspect ratio for better sensing performance, thinner ZnO nanowire (50–100 nm) was used than that (600 ± 100 nm) in the previous work. All these make it more difficult to control the thickness of MOF thin film. All factors in the reaction, such as temperature, the ratio of *N*,*N*-Dimethylformamide (DMF) and water, the concentration of organic ligand and metal ion, were found to vary the final thickness of MOF sheath in ZnO@ZIF-CoZn nanostructure. After optimization, by fixing the reaction conditions with DMF and water in 13.5:2.5 ratio, 0.86×10^{-3} M $Co(NO_3)_2$ and at 60 °C, ZIF-CoZn thin film can be controlled to grow to required thickness by only changing the concentration of 2-methylimadazole (Hmim, details see the Supporting Information).

Figure 2a,e shows the morphological features of ZnO nanowire array with the length of 2–4 µm and the diameter of 50–100 nm, respectively. All the ZnO nanowires (Figure 2a,e) are single crystal and grow along [001] direction. After coated with a layer of ZIF-CoZn (Figure 2b–d,f–h), the nanowires keep standing vertically on the substrate with similar length. But their diameters become larger as increasing the thickness of ZIF-CoZn sheath. Scanning transmission electron microscopy (STEM) measurements (Figure S1, Supporting Information) clearly show the core–sheath structure of ZnO@ZIF-CoZn. ZnO core shows brighter contrast owing to larger atomic mass than that of MOF sheath (Figure S1c–e, Supporting Information). Although, it is not easy to clearly observe the sheath with only 5 and 15 nm in thickness, elemental maps of these samples demonstrate that Co and Zn do coexist in sheath. X-ray photoelectron spectroscopy (XPS) measurements further

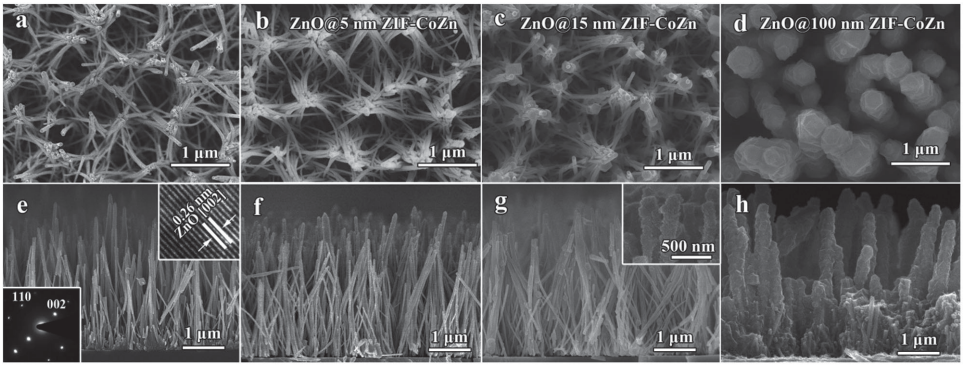

Figure 2. Plan and cross-sectional view of ZnO and ZnO@ ZIF-CoZn nanowire arrays: a,e) pure ZnO with high-resolution transmission microscopy (HRTEM) and selected-area electron diffraction (SAED) patterns of a single ZnO nanowire as inset; b,f) ZnO@5 nm ZIF-CoZn; c,g) ZnO@15 nm ZIF-CoZn with high-magnification SEM as inset; d,h) ZnO@100 nm ZIF-CoZn.

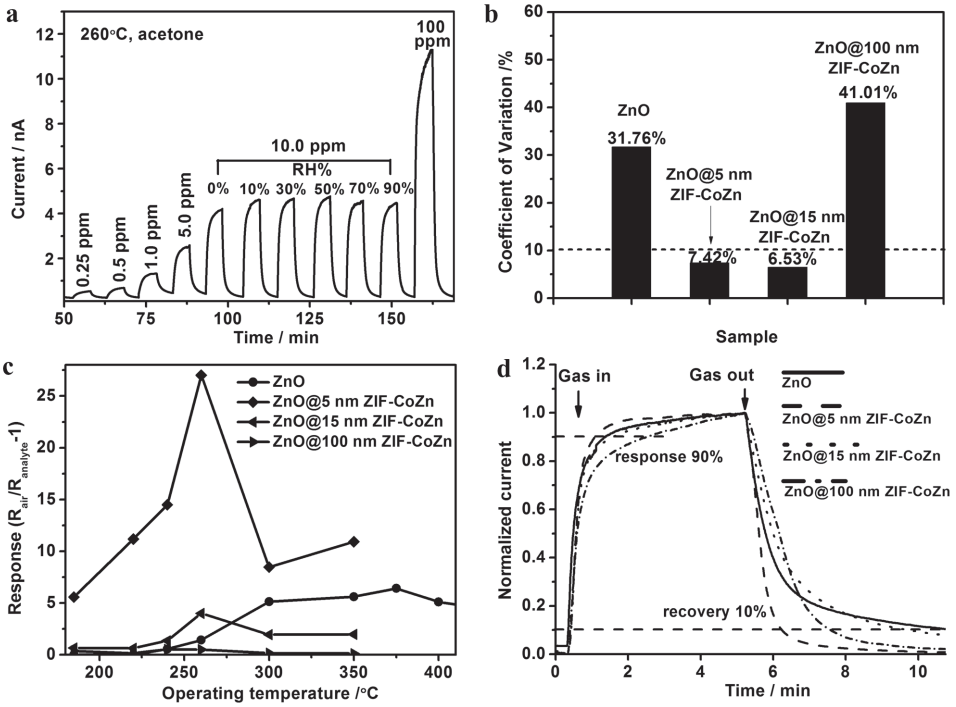

Figure 3. Gas sensing properties of ZnO@ZIF-CoZn sensor: a) response-recovery curves of ZnO@5 nm ZIF-CoZn to acetone with different concentrations in dry air and to 10 ppm acetone with different relative humidity; b) CV of the sensors by varying RH from 0% to 90% (acetone 10 ppm, 260 °C), c) temperature-dependent responses; d) response-recovery curves to 100 ppm acetone at 260 °C.

confirm the coexistence of Co and Zn but also show that the distribution of Co and Zn in ZIF-CoZn sheath is not homogenous (Figure S2, Supporting Information). It has been known that XPS is a surface-sensitive quantitative spectroscopic technique. Normally it can detect the elements as deep as 10 nm from the surface. Moreover, XPS measurements reveal that both metals are 2+. This valence is just right for compensating the negative charge of Hmim ligand in ZIF-CoZn, which can also be found in ZIF-8(Zn) and ZIF-67(Co).[14] N1s peak of ZIF-CoZn sheath located between those of ZIF-8(Zn) and ZIF-67(Co) (Figure S2d, Supporting Information), which indicates the coexistence of Co—N and Zn—N bonds in ZIF-CoZn. In addition, the order of N1s binding energy, Co-ZIF < ZnO@100 nm ZIF-CoZn < ZnO@15 nm ZIF-CoZn < Zn-ZIF indicates that the ratio of Co^{2+} to Zn^{2+} on the surface of ZIF-CoZn sheath increased with increasing the thickness of sheath. This may be due to the concentration gradient of Zn^{2+} from the surrounding of ZnO nanowire to reaction solution during synthesis. The peaks of ZnO@ZIF-CoZn in powder X-ray diffraction (PXRD) before 20° are very similar to these of ZIF-8(Zn) and ZIF-67(Co) (Figure S3, Supporting Information), which demonstrates that ZIF-CoZn is isostructural with ZIF-8(Zn) and ZIF-67(Co).[13,15] Besides the peaks of ZIF-CoZn, other peaks in PXRD pattern could be assigned to wurtzite ZnO (Joint Committee on Powder Diffraction Standards, JCPDS Card No. 01-075-1526) and sapphire substrate (Figure S3b, Supporting Information). As the thickness of sheath increases, the intensity of the diffraction peaks of ZIF-CoZn also increases that further confirms the results of scanning electron microscopy (SEM), TEM, and XPS analysis.

Gas sensing performance of ZnO@ZIF-CoZn sensor was evaluated with ZnO nanowire array-based sensor as control sample. The experiments were carried out by placing the sensor device in a sealed quartz chamber of tube furnace and monitoring the resistance of the device in diluted acetone with dry air as carrier gas (Figure S4, Supporting Information). **Figure 3**a shows the typical dynamic response of ZnO@ZIF-CoZn sensor to acetone with different concentration in dry air and to 10 ppm acetone under different relative humidity (RH) as interference. The current curve of ZnO@ZIF-CoZn sensor presents good response recovery to a broad range of the acetone concentrations (0.25–100 ppm). Notably, after coating with a layer of ZIF-CoZn, the selectivity between acetone and humidity of ZnO-based sensor has been significantly improved.

The coefficient of variation (CV) is used to represent the effect of humidity on responses, which is defined as

$$CV = R_{SD}/R_{average} \times 100\% \quad (1)$$

where R_{SD} and $R_{average}$ are the standard deviation (SD) and average value of responses with different humidity, respectively. The higher CV value means the worse antiinterference performance. At 10 ppm acetone, the responses of the ZnO@5 nm ZIF-CoZn device only varies 7.42% (CV) when changing RH from 0% to 90% (Figure 3a,b). Comparatively, ZnO nanowire array sensor shows a variation as high as 31.76% at the same conditions (Figure 3b). To increase the thickness of ZIF-CoZn thin film from 5 to 15 nm would further decrease the CV to 6.53%. However, when further increasing ZIF-CoZn thin film

to 100 nm, the selectivity of the device becomes worse and CV as huge as 41.01% was observed.

The sensor response in this work is defined as the ratio of sensor resistance in air (R_{air}) and in analytic gas ($R_{analyte}$):

$$\text{Response} = R_{air}/R_{analyte} - 1 \quad (2)$$

Response-concentration log–log plots show good linearity for all sensors, based on which the detection limit of each sensor can be deduced by setting Response = 0.1 (Figure S5, Supporting Information). ZnO@5 nm ZIF-CoZn device has the best detection limit in all devices, which is down to trace level with the value of 0.0019 ppm. The detection limits of the devices in this work are in the order of ZnO@5 nm ZIF-CoZn < ZnO@15 nm ZIF-CoZn < ZnO < ZnO@100 nm ZIF-CoZn. Compared with ZnO nanowire array sensor, ZnO@5 nm ZIF-CoZn has improved the detection limit by almost 2 orders of magnitude (**Table 1**) and this value is comparable with that of noble metal decorated ZnO gas sensors working at higher temperature (Table S2, Supporting Information).

In order to optimize the operating temperature for best sensing response, ZnO@ZIF-CoZn sensors were evaluated from 200 to 350 °C in 10 ppm acetone atmosphere (Figure 3c). Compared with ZnO nanowire array sensor which has optimal operating temperature around 375 °C in this work, ZIF-CoZn thin film coating decrease the optimal operating temperature of the sensors to 240–260 °C. Notably, the response of ZnO@5 nm ZIF-CoZn sensor to 10 ppm acetone is up to 27 even at 260 °C, which is ≈20 times higher than that of pure ZnO nanowire array (only 1.5). Moreover, the response of ZnO@5 nm ZIF-CoZn sensor to 100 ppm acetone is much higher than that of noble metal decorated ZnO sensors and comparable to the best reported ZnO-based sensor (Table S2, Supporting Information).

The response time of the sensor is the time required increasing the current to 90% of the saturation value and the recovery time is the time required decreasing the saturated current to its 10%. Figure 3d illustrates the response and recovery characteristic curves of the sensors based on instantaneous supply and cutoff of 100 ppm acetone in a 10 min cycle. ZnO@5 nm ZIF-CoZn shows the shortest response and recovery times in all sensors of this work with the values of 0.72 and 1.02 min, respectively. Compared with ZnO nanowire array sensor, the response and recovery of ZnO@5 nm ZIF-CoZn speed up by 48% and 470%, respectively.

ZnO@5 nm ZIF-CoZn also shows good response repeatability and recyclability to acetone (for details see Figure S6, Supporting Information). After continuously working for 1 week, the sensor can still keep CV less than 10%. Moreover, besides acetone, ZnO@ZIF-CoZn sensor shows responses to many other VOCs and gases (Figure S7, Supporting Information), which makes it possible to use ZnO@ZIF-CoZn to solve the humidity problem in detecting these analytes.

Vapor sorption measurements confirm that porous ZIF-CoZn (Co:Zn = 1:1 in mole) can selectively adsorb acetone rather than water (Figure S8a, Supporting Information). PXRD patterns show that this sample has the same crystal structure as that of ZIF-8(Zn) and ZIF-67(Co) (Figure S8b, Supporting Information). ZIF-CoZn coating on the surface of ZnO nanowire can serve as a filtration membrane to allow acetone molecule in and refuse the entry of water molecule due to its hydrophobic nature. So, ZnO@ZIF-CoZn-based sensors show good selectivity between acetone and humidity (Figure 3a,b). The poor antihumidity of ZnO@100 nm ZIF-CoZn as shown in Figure 3b can be explained by the competition response of n-type ZnO core and p-type CoO_x sheath. It has been mentioned above that ZIF-CoZn, ZIF-8(Zn) and ZIF-67(Co) are isostructural. However, the thermogravimetric analysis - differential thermal analysis (TG-DTA) measurements of these three samples show that the more Zn content in the crystal structure would result the better thermal stability (Figure S8c, Supporting Information). Therefore, ZIF-8 (Zn) shows the highest thermal stability and keeps intact until 330 °C and ZIF-67 (Co) shows the worst thermal stability and can only keep its structure to 220 °C, while ZIF-CoZn has medium thermal stability between 220 and 330 °C. On the other hand, it can be observed from XPS measurements that with the thickness of MOF thin film increase, Co:Zn ratio on the surface of MOF thin film also increases (Figure S3, Supporting Information). Therefore, 100 nm ZIF-CoZn coating has the worst thermal stability than 5 and 15 nm ones. After measured at 260 °C, ZnO@100 nm ZIF-CoZn shows its color changes from purple to black which is due to the pyrolysis of ZIF-CoZn to form CoO_x nanoparticles, which can be confirmed by TEM measurement (Figure S9, Supporting Information). As known, CoO_x is a typical p-type semiconductor and can be used as active material for detecting acetone.[14a,16] But similar to other MOX, CoO_x is also sensitive to humidity (Figure S10, Supporting Information). Meanwhile, the competition of n-type ZnO core and continuous p-type CoO_x sheath of ZnO@100 nm ZIF-CoZn decrease its response as observed in Figure 3c,d. Increasing ZIF-CoZn coating thicker to become a continuous thin film would even turn the device from n-type into p-type (Figure S11, Supporting Information) which completely destroys the selectivity of the sensor. Notably,

Table 1. Summarized sensing properties of ZnO and ZnO@5 nm ZIF-CoZn sensors.

Sample	Response	Antihumidity CV [%]	t_{res} [a] [min]	t_{rec} [b] [min]	Detection limit [ppm]	Operating temperature [°C]
ZnO	1.5	Poor	1.07	5.82	0.1666	375
ZnO@5nm ZIF-CoZn (this work)	27	Excellent	0.72	1.02	0.0019	260
Enhanced	≈20 times	_	48%	470%	100 times	120

[a] t_{res}, reponse time; [b] t_{rec}, recovery time.

after annealed at 400 °C for 2 h, 5 nm ZIF-CoZn was also decomposed and its device exhibited very poor response and antihumidity (CV = 49.00%) to 10 ppm acetone (Figure S12, Supporting Information). This observation further confirms the existence and the functions of MOF coating in ZnO@5 nm ZIF-CoZn.

The sensing property of MOX depends on the oxidation reaction between adsorbed oxygen species (such as O_2^-, O_2^{2-}, and O^-) and analyte on its surface. The produced electron from above oxidation is injected to the conduction band of MOX to change its conductivity. As shown in Figure 3c, with temperature increases from ambient, more oxygen species are activated for oxidation reaction due to the additional thermal energy and thus higher temperature results higher response.[17] Further to increase temperature beyond a certain optimum one, the reactants and oxygen species on the surface of ZnO begin to desorb significantly which leads to a decrease of sensing response.[18] The balance between above two process results the optimum temperature for the sensors in this work. Different from Zn^{2+} in ZIF-8(Zn), Co^{2+} in ZIF-CoZn has good catalytic property at 200–300 °C, which can dissociate and activate oxygen molecule from air then generate active oxygen species to help the catalytic oxidation of acetone.[19] Therefore, compared with ZnO and ZnO@ZIF-8(Zn), ZnO@ZIF-CoZn performed better activity and higher sensitivity to acetone and can work at lower temperature as shown in Figure 3c and Figure S13 (Supporting Information). The excellent catalytic effects of Co^{2+} also contribute to the accelerated response and recovery behavior of the device.[19] However, increasing the thickness of ZIF-CoZn would slow down the diffusion of acetone and oxygen to ZnO surface. So, ZnO@15 nm ZIF-CoZn sensor shows slower response behavior than ZnO@5 nm ZIF-CoZn. Further increasing the thickness of ZIF-CoZn to 100 nm results in much slower response and recovery due to fierce competition of n-type ZnO and p-type CoO_x.

In summary, a new material design strategy has been proposed to improve the selectivity and other performances of metal oxide-based chemiresistor gas sensor. Accordingly, MOX@catalytic MOF core–sheath nanowire array was successfully created as a sensing material for the first time. The gas sensor based on this new material shows significantly enhanced performances compared with the MOX sensor without MOF sheath: (1) the selectivity between acetone and humidity with standard deviation only 7.4% was achieved in large relative humidity range for the first time; (2) the response was enhanced ≈20 times; (3) the detection limit was improved by ≈2 orders of magnitude; (4) the response and recovery behaviors were accelerated by 48 and 470%, respectively; and (5) the operating temperature was decreased by ≈125 °C. Notably, MOF material has great designability on its structure and properties, unique gas selectivity on size, shape, chirality, etc. as well as excellent catalytic activity. Given these, the sensor device based on new material designed by above combining MOX and MOF strategy offers a high possibility to achieve the detecting on a single gas. In future, new material might simplify the structure and decrease the cost of the present gas sensor to adapt it to be further applied to wearable devices, intelligent automobile, smart electrical home appliances, and other precise detection fields.

Experimental Section

Preparation of ZnO@ZIF-CoZn Nanowire Array: ZnO nanowire array was grown on a sapphire substrate by a seeded method.[20] Then, ZnO nanowire array was immersed in 16 mL mixture of 13.5 mL *N*,*N*-dimethylformamide and 2.5 mL deionized water containing 0.004 g $Co(NO_3)_2{\cdot}6H_2O$ (0.86×10^{-3} M) and 0.040 g 2-methylimidazole (30.4×10^{-3} M) at 60 °C for 2 h to grow the ZIF-CoZn sheath. After that, ZnO@ZIF-CoZn nanowire array was washed repeatedly with deionized water and ethanol and dried in air at room temperature. Detailed experimental information and characterization can be found in the Supporting Information.

Gas Sensor Characterization: The sensor characterization was conducted by a home-made system.[21] Analyte gas was introduced into the quartz tube via mass flow controllers. The constant flow was 600 mL min^{-1}, the bias on the sensor was 5 V, and the current was recorded using Keithley 4200 Sourcemeter.

Supporting Information

Supporting Information is available from Wiley Online Library or from the author.

Acknowledgements

This work was supported by the National Natural Science Foundation of China (51402293, 21401193, and 21550110194), the Natural Science Foundation of Fujian (2015J01230), and The Fund for Returned Overseas Chinese Scholars Sponsored by Ministry of Human Resources and Social Security of Fujian Province.

Received: December 30, 2015
Revised: March 16, 2016
Published online: May 6, 2016

[1] a) Z. Zhao, J. Tian, Y. Sang, A. Cabot, H. Liu, *Adv. Mater.* **2015**, *27*, 2557; b) T. Wagner, S. Haffer, C. Weinberger, D. Klaus, M. Tiemann, *Chem. Soc. Rev.* **2013**, *42*, 4036.

[2] a) N. S. Ramgir, Y. Yang, M. Zacharias, *Small* **2010**, *6*, 1705; b) P.-X. Gao, Y. Ding, Z. L. Wang, *Nano Lett.* **2009**, *9*, 137.

[3] a) H.-J. Kim, H.-M. Jeong, T.-H. Kim, J.-H. Chung, Y. C. Kang, J.-H. Lee, *ACS Appl. Mater. Interfaces* **2014**, *6*, 18197; b) L. Li, C. Zhang, W. Chen, *Nanoscale* **2015**, *7*, 12133; c) F. Röck, N. Barsan, U. Weimar, *Chem. Rev.* **2008**, *108*, 705.

[4] a) H.-J. Kim, J.-H. Lee, *Sens. Actuators, B* **2014**, *192*, 607; b) C. Wang, L. Yin, L. Zhang, D. Xiang, R. Gao, *Sensors* **2010**, *10*, 2088; c) N. Ma, K. Suematsu, M. Yuasa, T. Kida, K. Shimanoe, *ACS Appl. Mater. Interfaces* **2015**, *7*, 5863.

[5] a) G. B. Gardner, D. Venkataraman, J. S. Moore, S. Lee, *Nature* **1995**, *374*, 792; b) H. K. Chae, D. Y. Siberio-Pérez, J. Kim, Y. Go, M. Eddaoudi, A. J. Matzger, M. O'Keeffe, O. M. Yaghi, *Nature* **2004**, *427*, 523; c) S. Shimomura, M. Higuchi, R. Matsuda, K. Yoneda, Y. Hijikata, Y. Kubota, Y. Mita, J. Kim, M. Takata, S. Kitagawa, *Nat. Chem.* **2010**, *2*, 633; d) G. Férey, C. Mellot-Draznieks, C. Serre, F. Millange, J. Dutour, S. Surblé, I. Margiolaki, *Science* **2005**, *309*, 2040; e) Z. Chang, D. H. Yang, J. Xu, T. L. Hu, X. H. Bu, *Adv. Mater.* **2015**, *27*, 5432.

[6] a) K. J. Erickson, F. Léonard, V. Stavila, M. E. Foster, C. D. Spataru, R. E. Jones, B. M. Foley, P. E. Hopkins, M. D. Allendorf, A. A. Talin, *Adv. Mater.* **2015**, *27*, 3453; b) J. M. Taylor, T. Komatsu, S. Dekura, K. Otsubo, M. Takata, H. Kitagawa, *J. Am. Chem. Soc.* **2015**, *137*,

11498; c) G. K. H. Shimizu, J. M. Taylor, S. Kim, *Science* **2013**, *341*, 354; d) Y.-Z. Chen, Y.-X. Zhou, H. Wang, J. Lu, T. Uchida, Q. Xu, S.-H. Yu, H.-L. Jiang, *ACS Catal.* **2015**, *5*, 2062; e) Q.-G. Zhai, C. Mao, X. Zhao, Q. Lin, F. Bu, X. Chen, X. Bu, P. Feng, *Angew. Chem. Int. Ed.* **2015**, *54*, 7886; f) X. Xu, Z. Zhang, X. Wang, *Adv. Mater.* **2015**, *27*, 5365; g) S. R. Batten, R. Robson, *Angew. Chem. Int. Ed.* **1998**, *37*, 1460; h) M.-H. Zeng, Z. Yin, Y.-X. Tan, W.-X. Zhang, Y.-P. He, M. Kurmoo, *J. Am. Chem. Soc.* **2014**, *136*, 4680; i) L. E. Darago, M. L. Aubrey, C. J. Yu, M. I. Gonzalez, J. R. Long, *J. Am. Chem. Soc.* **2015**, *137*, 15703; j) Q. Zhang, J. Su, D. Feng, Z. Wei, X. Zou, H.-C. Zhou, *J. Am. Chem. Soc.* **2015**, *137*, 10064; k) Y. Cui, R. Song, J. Yu, M. Liu, Z. Wang, C. Wu, Y. Yang, Z. Wang, B. Chen, G. Qian, *Adv. Mater.* **2015**, *27*, 1420.

[7] a) E.-X. Chen, H. Yang, J. Zhang, *Inorg. Chem.* **2014**, *53*, 5411; b) E.-X. Chen, H.-R. Fu, R. Lin, Y.-X. Tan, J. Zhang, *ACS Appl. Mater. Interfaces* **2014**, *6*, 22871; c) J. Teufel, H. Oh, M. Hirscher, M. Wahiduzzaman, L. Zhechkov, A. Kuc, T. Heine, D. Denysenko, D. Volkmer, *Adv. Mater.* **2013**, *25*, 635; d) B. R. Pimentel, A. Parulkar, E.-K. Zhou, N. A. Brunelli, R. P. Lively, *ChemSusChem* **2014**, *7*, 3202; e) J. J. Gassensmith, J. Y. Kim, J. M. Holcroft, O. K. Farha, J. F. Stoddart, J. T. Hupp, N. C. Jeong, *J. Am. Chem. Soc.* **2014**, *136*, 8277.

[8] S. Achmann, G. Hagen, J. Kita, I. M. Malkowsky, C. Kiener, R. Moos, *Sensors* **2009**, *9*, 1574.

[9] M. G. Campbell, S. F. Liu, T. M. Swager, M. Dincă, *J. Am. Chem. Soc.* **2015**, *137*, 13780.

[10] a) M. G. Campbell, D. Sheberla, S. F. Liu, T. M. Swager, M. Dincă, *Angew. Chem. Int. Ed.* **2015**, *54*, 4349; b) D. J. Wales, J. Grand, V. P. Ting, R. D. Burke, K. J. Edler, C. R. Bowen, S. Mintova, A. D. Burrows, *Chem. Soc. Rev.* **2015**, *44*, 4290; c) V. Pentyala, P. Davydovskaya, M. Ade, R. Pohle, G. Urban, *Sens. Actuators, B* **2016**, *222*, 904.

[11] a) D. H. Kim, Y. S. Shim, J.-M. Jeon, H. Y. Jeong, S. S. Park, Y.-W. Kim, J. S. Kim, J.-H. Lee, H. W. Jang, *ACS Appl. Mater. Interfaces* **2014**, *6*, 14779; b) M. Righettoni, A. Tricoli, S. E. Pratsinis, *Chem. Mater.* **2010**, *22*, 3152.

[12] S. K. Kundu, J. A. Bruzek, R. Nair, A. M. Judilla, *Clin. Chem.* **1993**, *39*, 87.

[13] W. W. Zhan, Q. Kuang, J. Z. Zhou, X. J. Kong, Z. X. Xie, L. S. Zheng, *J. Am. Chem. Soc.* **2013**, *135*, 1926.

[14] a) Y. Lu, W. Zhan, Y. He, Y. Wang, X. Kong, Q. Kuang, Z. Xie, L. Zheng, *ACS Appl. Mater. Interfaces* **2014**, *6*, 4186; b) H. Chen, L. Wang, J. Yang, R. T. Yang, *J. Phys. Chem. C* **2013**, *117*, 7565.

[15] a) Q. Shi, Z. Chen, Z. Song, J. Li, J. Dong, *Angew. Chem.* **2011**, *123*, 698; b) X. Liu, L. He, J. Zheng, J. Guo, F. Bi, X. Ma, K. Zhao, Y. Liu, R. Song, Z. Tang, *Adv. Mater.* **2015**, *27*, 3273.

[16] L. Li, M. Liu, S. He, W. Chen, *Anal. Chem.* **2014**, *86*, 7996.

[17] a) M. Wagh, G. Jain, D. Patil, S. Patil, L. Patil, *Sens. Actuators, B* **2006**, *115*, 128; b) M. Yao, F. Ding, Y. Cao, P. Hu, J. Fan, C. Lu, F. Yuan, C. Shi, Y. Chen, *Sens. Actuators, B* **2014**, *201*, 255.

[18] H. Windischmann, P. Mark, *J. Electrochem. Soc.* **1979**, *126*, 627.

[19] a) G. Saracco, S. Vankova, C. Pagliano, B. Bonelli, E. Garrone, *Phys. Chem. Chem. Phys.* **2014**, *16*, 6139; b) J. Zakzeski, A. Dębczak, P. C. A. Bruijnincx, B. M. Weckhuysen, *Appl. Catal., A* **2011**, *394*, 79; c) L. Zhang, Z. Su, F. Jiang, L. Yang, J. Qian, Y. Zhou, W. Li, M. Hong, *Nanoscale* **2014**, *6*, 6590.

[20] a) S. K. Youn, N. Ramgir, C. Wang, K. Subannajui, V. Cimalla, M. Zacharias, *J. Phys. Chem. C* **2010**, *114*, 10092; b) L. E. Greene, M. Law, D. H. Tan, M. Montano, J. Goldberger, G. Somorjai, P. D. Yang, *Nano Lett.* **2005**, *5*, 1231.

[21] M. Yao, P. Hu, Y. Cao, W. Xiang, X. Zhang, F. Yuan, Y. Chen, *Sens. Actuators, B* **2013**, *117*, 562.